

Alma Mater Studiorum Università di Bologna
Archivio istituzionale della ricerca

Extensive ro-vibrational analysis of deuterated-cyanoacetylene (DC3N) from millimeter-wavelengths to the infrared domain

This is the final peer-reviewed author's accepted manuscript (postprint) of the following publication:

Published Version:

Melosso M., Bizzocchi L., Adamczyk A., Cane' E., Caselli P., Colzi L., et al. (2020). Extensive ro-vibrational analysis of deuterated-cyanoacetylene (DC3N) from millimeter-wavelengths to the infrared domain. JOURNAL OF QUANTITATIVE SPECTROSCOPY & RADIATIVE TRANSFER, 254, 1-9 [10.1016/j.jqsrt.2020.107221].

Availability:

This version is available at: <https://hdl.handle.net/11585/778698> since: 2022-02-28

Published:

DOI: <http://doi.org/10.1016/j.jqsrt.2020.107221>

Terms of use:

Some rights reserved. The terms and conditions for the reuse of this version of the manuscript are specified in the publishing policy. For all terms of use and more information see the publisher's website.

This item was downloaded from IRIS Università di Bologna (<https://cris.unibo.it/>).
When citing, please refer to the published version.

(Article begins on next page)

This is the final peer-reviewed accepted manuscript of:

Melosso, M., Bizzocchi, L., Adamczyk, A., Canè, E., Caselli, P., Colzi, L., Dore, L., Giuliano, B.M., Guillemin, J.-C., Martin-Drumel, M.-A., Pirali, O., Pietropolli Charmet, A., Prudenzano, D., Rivilla, V.M., Tamassia, F., 2020. Extensive ro-vibrational analysis of deuterated-cyanoacetylene (DC3N) from millimeter-wavelengths to the infrared domain. *Journal of Quantitative Spectroscopy and Radiative Transfer* 254, 107221.

The final published version is available online at:
<https://doi.org/10.1016/j.jqsrt.2020.107221>

Rights / License:

The terms and conditions for the reuse of this version of the manuscript are specified in the publishing policy. For all terms of use and more information see the publisher's website.

This item was downloaded from IRIS Università di Bologna (<https://cris.unibo.it/>)

When citing, please refer to the published version.

Extensive ro-vibrational analysis of deuterated-cyanoacetylene (DC₃N) from millimeter-wavelengths to the infrared domain

Mattia Melosso^{a,*}, Luca Bizzocchi^b, Aleksandra Adamczyk^c, Elisabetta Canè^c, Paola Caselli^b, Laura Colzi^d, Luca Dore^a, Barbara M. Giuliano^b, Jean-Claude Guillemin^e, Marie-Aline Martin-Drumel^f, Olivier Pirali^{f,g}, Andrea Pietropoli Charmet^h, Domenico Prudenzeno^b, Víctor M. Rivilla^d, Filippo Tamassia^{c,*}

^a*Dipartimento di Chimica “Giacomo Ciamician”, Università di Bologna, Via F. Selmi 2, 40126 Bologna (Italy)*

^b*Center for Astrochemical Studies, Max Planck Institut für extraterrestrische Physik Gießenbachstraße 1, 85748 Garching bei München (Germany)*

^c*Dipartimento di Chimica Industriale “Toso Montanari”, Università di Bologna, Viale del Risorgimento 4, 40136 Bologna (Italy)*

^d*INAF-Osservatorio Astrofisico di Arcetri, Largo Enrico Fermi 5, 50125, Firenze (Italy)*

^e*Univ Rennes, Ecole Nationale Supérieure de Chimie de Rennes, CNRS, ISCR-UMR6226, 35000 Rennes (France)*

^f*Université Paris-Saclay, CNRS, Institut des Sciences Moléculaires d’Orsay, 91405 Orsay (France)*

^g*SOLEIL Synchrotron, AILES beamline, L’Orme des Merisiers, Saint-Aubin, 91190 Gif-sur-Yvette, (France)*

^h*Dipartimento di Scienze Molecolari e Nanosistemi, Università Ca’ Foscari Venezia, Via Torino 155, 30172 Mestre (Italy)*

Abstract

Cyanoacetylene, the simplest cyanopolyne, is an abundant interstellar molecule commonly observed in a vast variety of astronomical sources. Despite its importance as a potential tracer of the evolution of star-forming processes, the deuterated form of cyanoacetylene is less observed and less studied in the laboratory than the main isotopologue. Here, we report the most extensive spectroscopic characterization of DC₃N to date, from the millimeter domain to the infrared region. Rotational and ro-vibrational spectra have been recorded using millimeter-wave frequency-modulation and Fourier-transform infrared spectrometers, respectively. All the vibrational states with energy up to 1015 cm⁻¹ have been analyzed in a combined fit, where the effects due to anharmonic resonances have been adequately accounted for. The analysis contains over 6500 distinct transition frequencies, from which all the vibrational energies have been determined with good precision for many fundamental, overtone, and combination states. This work provides a comprehensive line catalog for astronomical observations of DC₃N.

Keywords: Cyanoacetylene, Interstellar species, Ro-vibrational spectroscopy, Spectral analysis, Anharmonic resonances, Line catalog

1. Introduction

Highly unsaturated molecules account for a large portion of the known interstellar species [1]. For instance, the presence of several carbon-chain molecules is one of the most characteristic features of the chemical composition of starless cores, such as the Taurus Molecular Cloud (TMC-1), one of the brightest source of carbon-chain species [2]. Among the unsaturated molecular species, cyanopolyynes, i.e., linear molecules of general chemical formula HC_{2n+1}N, are widespread in the interstellar medium (ISM) and all members up to HC₁₁N have been detected to date [3]. Cyanoacetylene (HC₃N, IUPAC name prop-2-ynenitrile), the simplest member of the cyanopolyynes family, was found to be an abundant species in a large variety of astronomical objects: starless cores [4], post-AGB objects [5], carbon-rich circumstellar envelopes

^{*}Supplementary material available.

^{*}Corresponding authors

Email addresses: mattia.melosso2@unibo.it (Mattia Melosso), filippo.tamassia@unibo.it (Filippo Tamassia)

10 [6], massive star-forming regions [7], protoplanetary disks [8], solar-type protostars [9], external galaxies [10],
11 and Galactic Center molecular clouds [11].

12 The deuterated form of cyanoacetylene (DC₃N) has been detected in the ISM as well. The first astronom-
13 ical observation of DC₃N has been reported towards TMC-1 [12] by the detection of the $J = 5 \rightarrow 4$ emission
14 rotational transition around 42 GHz. Consecutively, DC₃N has tentatively been detected in the high-mass
15 star-forming regions Orion KL [13] and Sagittarius B2 [14]. In these regions, deuterium fractionation is not
16 as effective as in dark clouds, thus preventing a strong enhancement above the deuterium cosmic abundance.
17 Recently, DC₃N has been detected in some low-mass cores (see e.g., Refs. [9], [15]) and in a sample of 15 high-
18 mass star-forming cores [16]. The latter work, based on the spectroscopic results presented in this paper,
19 suggests that DC₃N is enhanced in the cold and outer regions of star-forming regions, likely indicating the
20 initial deuteration level of the large-scale molecular cloud within which star formation takes place. Rivilla
21 *et al.* [16] also summarize all the astronomical observations of DC₃N so far.

22 Microwave (MW) transitions of DC₃N were first reported for the ground and the four lowest singly-
23 excited states during the course of an extensive study of cyanoacetylene isotopologues [17]. A larger number
24 of vibrationally excited states was re-examined in depth some years later and a rigorous determination of
25 the effective molecular parameters was attained [18]. Recently, the laboratory investigation of the rotational
26 spectrum of DC₃N has been extended to the THz regime for the ground and the $\nu_7 = 1$ states [19]. In the
27 same paper, the authors revised the ¹⁴N and D hyperfine-structure constants derived in Refs. [20, 21] from
28 supersonic-jet Fourier-Transform Microwave (FT-MW) spectroscopy.

29 As far as its infrared (IR) spectrum is concerned, the experimental position and intensity of all funda-
30 mentals but the weak ν_4 mode have been determined from low resolution (0.5 cm^{-1}) studies [22, 23]. Some
31 combination and overtone bands were also observed in the same works. In addition, two medium resolution
32 ($0.025\text{--}0.050 \text{ cm}^{-1}$) IR studies were performed by Mallinson & Fayt [24] and Couveliers *et al.* [25]. In the
33 former, the band center of the three stretching modes of DC₃N (ν_1 , ν_2 , and ν_3) has been determined; in
34 the latter, the far-infrared (FIR) spectrum was recorded between 200 and 365 cm^{-1} and the ν_7 fundamental
35 was analyzed together with the bands $\nu_6 - \nu_7$, $\nu_5 - \nu_7$, and $\nu_4 - \nu_6$, and their hot-bands.

36 In this work, a detailed investigation of both millimeter/submillimeter-wave and infrared spectra of
37 DC₃N is reported. Pure rotational transitions within all the vibrational states with energy lower than
38 1015 cm^{-1} have been detected and 27 fundamental, overtone, combination, and hot ro-vibrational bands
39 have been analyzed at high resolution ($0.001\text{--}0.01 \text{ cm}^{-1}$). The new measurements have been combined in
40 a fit containing almost 6700 distinct transition frequencies, thus allowing the determination of a consistent
41 set of spectroscopic parameters. This work represents the most exhaustive spectroscopic characterization
42 of DC₃N so far and provides a robust line catalog useful for astronomical applications. Moreover, the large
43 number of vibrational excited states are of interest for harmonic/anharmonic force field computations.

44 The paper is structured as follows. First, the synthesis of the sample and the spectrometers used
45 for spectral recording are described (§2). Then, the effective Hamiltonian employed for the energy levels
46 description is given (§3). Successively, the general features of the spectra and their analysis are discussed
47 (§4). Finally, the results are summarized and the conclusions are presented (§5).

48 2. Experimental details

49 2.1. Synthesis of deuterocyanoacetylene

50 Methyl propiolate (HC≡CCOOCH₃) was purchased from TCI-Europe and used without further purifi-
51 cation. The DC₃N sample was synthesized in Rennes following the procedure described in Ref. [23]. Briefly,
52 HC≡CCOOCH₃ was added dropwise to liquid ammonia resulting in a 100 % conversion into HC≡CCONH₂.
53 The propiolamide was then mixed with phosphorous anhydride (P₄O₁₀) and calcined white sand; the whole
54 system was heated up to 470 K over 2 h while connected to a liquid nitrogen-cooled trap where pure
55 cyanoacetylene was collected. Cyanoacetylene (3 g), heavy water (D₂O, 4 mL) and potassium carbonate
56 (K₂CO₃, 50 mg) were mixed together in an inert atmosphere. The biphasic mixture was then stirred for
57 about 20 min at room temperature. Subsequently, on a vacuum line, partially deuterated cyanoacetylene
58 was condensed in a 77 K cooled trap, while water was blocked in a first 220 K trap. The operation was

59 repeated 3 times by addition of D₂O and K₂CO₃ to the partially deuterated cyanoacetylene. The residual
60 D₂O was removed by vaporisation on P₄O₁₀ and DC₃N was finally condensed in a trap cooled to 150 K.
61 Deuterocyanoacetylene with an isotopic purity greater than 98 % was obtained in a 67 % yield. The sample
62 can be stored indefinitely at 250 K without decomposition.

63 2.2. Infrared spectrometers

64 The FIR spectrum of DC₃N was recorded at the AILES beamline of the SOLEIL synchrotron facility
65 using a Bruker IFS 125 FT interferometer [26] and a white-type multipass absorption cell whose optics
66 were adjusted to obtain a 150 m optical path length [27, 28]. For the present experiment, we used the far-
67 IR synchrotron radiation continuum extracted by the AILES beamline. The interferometer was equipped
68 with a 6 μm Mylar-composite beamsplitter and a 4 K cooled Si-bolometer. Two 50 μm-thick polypropylene
69 windows isolated the cell from the interferometer, which was continuously evacuated to 0.01 Pa limiting
70 the absorption of atmospheric water. Vapor of DC₃N was injected into the absorption cell at a 25 Pa
71 pressure. The spectrum covers the range 70–500 cm⁻¹ and consists of the co-addition of 380 scans recorded
72 at 0.00102 cm⁻¹ resolution.

73 IR spectra in the 450–1600 cm⁻¹ range were recorded in Bologna using a Bomem DA3.002 Fourier-
74 Transform spectrometer [29]. It was equipped with a Global source, a KBr beamsplitter, and a liquid
75 nitrogen-cooled HgCdTe detector. A multi-pass cell with absorption-lengths from 4 to 8 m was employed
76 for the measurements. Sample pressures ranging between 25 and 650 Pa were used to record the spectra.
77 The resolution was generally 0.004 cm⁻¹, except for the very weak ν₄ band, which was recorded at a lower
78 resolution of 0.012 cm⁻¹. Several hundreds of scans, typically 800, were co-added in order to improve the
79 signal-to-noise ratio (S/N) of the spectra.

80 All the spectra have been calibrated using residual water or CO₂ absorption lines whose reference
81 wavenumbers were taken from Refs. [30, 31] and from HITRAN [32], respectively. No apodization functions
82 were applied to the interferograms.

83 2.3. Millimeter and submillimeter spectrometers

84 Rotational spectra have been recorded using two frequency-modulation (FM) millimeter/submillimeter
85 spectrometers located in Bologna and in Garching.

86 The Bologna spectrometer has been described in details elsewhere [33, 34]. Briefly, a Gunn diode oscillator
87 operating in the W band (80–115 GHz) was used as primary source of radiation, whose frequency and phase
88 stability are ensured by a Phase-Lock Loop (PLL). Spectral coverage at higher frequencies was obtained by
89 coupling the Gunn diode to passive frequency multipliers in cascade (doublers and triplers, Virginia Diodes,
90 Inc.). The output radiation, sine-wave modulated in frequency ($f = 48$ kHz), was fed to the glass absorption
91 cell containing DC₃N vapors at a pressure between 1 and 15 Pa, depending on the intensity of the lines
92 under consideration. The outgoing signal was detected by a Schottky barrier diode and sent to a Lock-in
93 amplifier set at twice the modulation-frequency ($2f$ scheme); the demodulated signal is then filtered into a
94 resistor-capacitor (RC) system before data acquisition.

95 In Garching the CASAC spectrometer developed at the Max-Planck-Institut für extraterrestrische Physik
96 was used. Full details on the experimental set-up are given in Ref. [35]; here, we report only a few key
97 details which apply to the present investigation. The instrument is equipped with an active multiplier chain
98 (Virginia Diodes) as a source of radiation in the 82–125 GHz band. Further multiplier stages in cascade
99 allow to extend the frequency coverage up to ~ 1.1 THz with an available power of 2–20 μW. The primary
100 millimeter radiation stage is driven by a cm-wave synthesizer (Keysight E8257D) operating in the 18–28 GHz
101 band, which is locked to a Rb atomic clock to achieve accurate frequency and phase stabilisation. A closed-
102 cycle He-cooled InSb hot-electron bolometer operating at 4 K (QMC) is used as a detector. As in Bologna,
103 frequency ($f = 50$ kHz) modulation technique is employed and the second derivative of the actual absorption
104 profile is thus recorded by the computer-controlled acquisition system after lock-in demodulation at $2f$. The
105 absorption cell is a plain Pyrex tube (3 m long and 5 cm in diameter) fitted with high-density polyethylene
106 windows. The measurement were performed using gaseous samples at pressure of a few Pa. In this condition,
107 DC₃N is stable for ca. 2 h without significant decomposition due to hydrogen exchange.

108 The spectra were recorded in the frequency ranges 80–115 GHz and 920–1070 GHz in Garching, and in
 109 the window 240–440 GHz in Bologna.

Table 1: Energy and intensity of all fundamental modes of DC₃N.

Modes	Description	Energy (cm ⁻¹)	Reference	Abs. intensity (atm ⁻¹ cm ⁻²)
ν_1	C–D stretching	2608.520(3)	[24]	81.3 ± 5.7^a
ν_2	C≡C stretching	2252.155(3)	[24]	50.5 ± 2.4^a
ν_3	C≡N stretching	1968.329(3)	[24]	38.7 ± 4.0^a
ν_4	C–C stretching	867.60(6)	This Work	$< 0.1^b$
ν_5	CCD bending	522.263933(7)	This Work	83.8 ± 4.7^a
ν_6	CCC bending	492.759896(7)	This Work	$106. \pm 8^a$
ν_7	CCN bending	211.550293(5)	This Work	0.89 ± 0.11^b

[a] From low-resolution integrated band-intensity measurements at 296 K (Ref. [23]). [b] From low-resolution integrated band-intensity measurements at 293 K (Ref. [22]).

110 3. Theoretical background

111 From a spectroscopic point of view, DC₃N is a closed-shell linear rotor. It has 7 vibrational modes:
 112 4 stretchings (ν_1 – ν_4 ; Σ symmetry) and 3 doubly-degenerated bendings (ν_5 – ν_7 ; Π symmetry). They are
 113 summarized in Table 1. In the present work, only the low-lying vibrational states (ν_4 , ν_5 , ν_6 , and ν_7 , with
 114 one of multiple quanta of excitation) have been investigated for two main reasons: (i) transitions associated
 115 to the lower energy states are of astrophysical interest, and (ii) some of the vibrational states are connected
 116 by a network of anharmonic resonances fully described within our chosen energy threshold of 1015 cm⁻¹;
 117 above this limit the states are either unperturbed or involved in higher-order resonances. Therefore, the
 118 stretching modes ν_1 , ν_2 , and ν_3 , lying above this threshold, have not been investigated. Conventionally, we
 119 labelled a given vibrational state with the notation $(v_4, v_5^{l_5}, v_6^{l_6}, v_7^{l_7})_{e/f}$, where l_t is the vibrational angular
 120 momentum quantum number associated to the bending mode t and the e/f subscripts indicate the parity
 121 of the symmetrized wave functions [36]. When the l_t and e/f labels are not indicated, we refer to all the
 122 possible sub-levels of a state.

123 The full ro-vibrational wave-function is then given by the ket $|v_4, v_5^{l_5}, v_6^{l_6}, v_7^{l_7}; J, k\rangle_{e/f}$. The vibrational
 124 part of the wave-function is expressed as combination of one- or two-dimensional harmonic oscillators,
 125 whereas the rotational part is the symmetric-top wave-function whose quantum number k is given by $k =$
 126 $l_5 + l_6 + l_7$. A substate is denoted as Σ when $k = 0$, Π for $|k| = 1$, Δ for $|k| = 2$, and so on.

127 The following Wang-type linear combinations [37] lead to symmetry-adapted basis functions:

$$|v_4, v_5^{l_5}, v_6^{l_6}, v_7^{l_7}; J, k\rangle_{e/f} = \frac{1}{\sqrt{2}} \left\{ |v_4, v_5^{l_5}, v_6^{l_6}, v_7^{l_7}; J, k\rangle \pm (-1)^k |v_4, v_5^{-l_5}, v_6^{-l_6}, v_7^{-l_7}; J, -k\rangle \right\}, \quad (1a)$$

$$|v_4, 0^0, 0^0, 0^0; J, 0\rangle_e = |v_4, 0^0, 0^0, 0^0; J, 0\rangle. \quad (1b)$$

128 The upper and lower signs (\pm) correspond to e and f wave-functions, respectively. For Σ states ($k = 0$),
 129 the first non-zero l_t is chosen positive. Here, the omission of the e/f label indicates unsymmetrised wave-
 130 functions. The Hamiltonian used to reproduce the ro-vibrational energy levels is equivalent to the one used

131 for HC₃N [38]:

$$\mathcal{H} = \mathcal{H}_{\text{rv}} + \mathcal{H}_{l\text{-type}} + \mathcal{H}_{\text{res}}, \quad (2)$$

132 where \mathcal{H}_{rv} is the ro-vibrational energy including centrifugal distortion corrections, $\mathcal{H}_{l\text{-type}}$ represents the
 133 l -type interaction between the l sub-levels of the excited bending states, and \mathcal{H}_{res} accounts for resonances
 134 among accidentally quasi-degenerate ro-vibrational states. The resonance network active in DC₃N resembles
 135 the one found for HC₃N and will be described later.

136 The Hamiltonian matrix is built by using unsymmetrised ro-vibrational functions. It is subsequently
 137 factorized and symmetrized using Eqs. (1). The matrix elements of the effective Hamiltonian are expressed
 138 using the formalism already employed for the analysis of HC₃N [38].

139 4. General features and analysis

140 4.1. Vibrational spectra

141 Although infrared spectra were recorded up to 1600 cm⁻¹ in this study, our analysis is limited to the
 142 portion of the electromagnetic spectrum below ~ 1040 cm⁻¹. This is because the highest energy state within
 143 our threshold of 1015 cm⁻¹ is the (0110) state, whose combination band falls in the region 999–1035 cm⁻¹.
 144 In total, 27 ro-vibrational bands have been observed at high resolution for the first time and successfully
 145 analyzed. They include fundamental, overtone, combination, and hot-bands, and are listed in Table 2 along
 146 with the observed sub-bands, frequency and J ranges, number of data used in the analysis, and the root-
 147 mean-square (*rms*) error of the final fit. All the observed bands are also graphically displayed in Figure 1

148 Figure 2 shows a general overview of portions of the FIR (180–460 cm⁻¹ range, upper panel) and mid-
 149 infrared (MIR, 450–800 cm⁻¹ range, bottom panel) spectra recorded in this work. The most prominent
 150 bands in the FIR region are the ν_7 fundamental, $\nu_6 - \nu_7$, $\nu_5 - \nu_7$, $\nu_4 - \nu_6$, and $2\nu_7$ overtone bands. The MIR
 151 region is dominated by the very strong fundamentals ν_6 and ν_5 . The low-frequency side of the spectrum
 152 is particularly crowded due to the proximity of the two fundamentals, the presence of their associated hot-
 153 bands, and of the ν_6 of HC₃N centered at 500 cm⁻¹. HC₃N is present in the sample as result of the H/D
 154 exchange in the cell.

155 Having a medium IR intensity, the combination bands $\nu_6 + \nu_7$ and $\nu_5 + \nu_7$ are well visible in the high-
 156 frequency part of the MIR spectrum as seen in the bottom panel of Figure 2. Although not displayed in
 157 Figure 2, the overtone $2\nu_6$ and the combination $\nu_5 + \nu_6$ bands centered around 975–1018 cm⁻¹ and 999–
 158 1035 cm⁻¹, respectively, are clearly detectable as well, despite the presence of strong absorption lines due to
 159 HDO. The very weak (< 0.1 atm⁻¹ cm⁻²) ν_4 fundamental at 830–865 cm⁻¹ had to be recorded at higher
 160 pressure (400 Pa) and lower resolution (0.012 cm⁻¹). In this case, up to 2600 scans were co-added to improve
 161 the S/N of the spectrum.

162 4.2. Rotational spectra

163 Rotational spectra were recorded for all the 14 states whose vibrational energy do not exceed our threshold
 164 of 1015 cm⁻¹. Literature data were available for some of these states, as pointed out in Section 1. However,
 165 line positions of some millimeter-wave transitions from Ref. [17] are affected by large uncertainties (up to
 166 300 kHz) and many data are limited to low frequencies. For these reasons, we decided to re-investigate
 167 and extend the spectrum for all these vibrational states. The largest improvements have been realized for
 168 the states (1000), (0110), (0020), and (0004) involved in a network of anharmonic resonances, for which
 169 extended data-sets were obtained. In particular, the (0110) state, not included in the analysis of Ref. [18],
 170 has been assigned for the first time in this study and its interaction with the (1000) state has been identified
 171 and properly accounted for.

172 Table 3 summarizes the set of rotational data used in the analysis, specifying the observed sub-levels,
 173 J and frequency ranges, number of distinct fitted frequencies, the *rms* error of the final fit, and the corre-
 174 sponding references used.

175 With the exception of $\nu_4 = 1$, all the states possess a rotational constant B greater than that of the
 176 ground state and therefore their rotational lines lie at frequencies higher than those of the corresponding

Table 2: Ro-vibrational bands recorded and analyzed in this work.

Band	Sub-bands	Freq. range (cm^{-1})	J range	No. of lines	$rms \times 10^4$ (cm^{-1})
ν_7	$\Pi - \Sigma^+$	190-240	1-93	258	0.5
ν_6	$\Pi - \Sigma^+$	466-522	2-109	267	3.6
ν_5	$\Pi - \Sigma^+$	500-557	0-117	255	3.7
ν_4	$\Sigma^+ - \Sigma^+$	830-865	0-61	109	9.6
$2\nu_7$	$\Sigma^+ - \Sigma^+$	405-445	2-78	136	1.0
$2\nu_6$	$\Sigma^+ - \Sigma^+$	975-1018	2-101	141	5.2
$\nu_6 + \nu_7$	$\Sigma^+ - \Sigma^+$	686-736	1-89	166	2.5
$\nu_5 + \nu_7$	$\Sigma^+ - \Sigma^+$	715-769	1-105	170	3.0
$\nu_5 + \nu_6$	$\Sigma^+ - \Sigma^+$	999-1035	3-63	102	3.8
$\nu_6 - \nu_7$	$\Pi - \Pi$	257-306	1-89	309	0.6
$\nu_5 - \nu_7$	$\Pi - \Pi$	288-333	1-86	291	0.7
$\nu_4 - \nu_6$	$\Sigma^+ - \Pi$	329-375	1-79	222	0.6
$4\nu_7 - \nu_6$	$\Sigma^+ - \Pi$	351-352	59-60	2	0.4
$2\nu_7 - \nu_7$	$\Sigma - \Pi$	193-236	1-78	391	0.8
$3\nu_7 - 2\nu_7$	$\Pi - \Sigma^+$	191-235	4-77	178	0.7
$4\nu_7 - 3\nu_7$	$\Sigma^+ - \Pi$	193-219	10-58	89	0.9
$3\nu_7 - \nu_7$	$\Pi - \Pi$	405-441	4-68	208	1.0
$\nu_6 + \nu_7 - \nu_7$	$(\Sigma, \Delta) - \Pi$	478-508	5-56	329	6.9
$\nu_6 + 2\nu_7 - 2\nu_7$	$\Pi - (\Sigma^+, \Delta)$	476-512	12-65	93	5.2
$2\nu_6 - \nu_6$	$\Sigma - \Pi$	500-519	10-68	43	7.0
$\nu_5 + \nu_7 - \nu_7$	$(\Sigma^+, \Delta) - \Pi$	505-545	2-75	464	4.5
$\nu_5 + 2\nu_7 - 2\nu_7$	$\Pi - (\Sigma, \Delta)$	505-542	2-82	106	3.5
$\nu_6 + 2\nu_7 - \nu_7$	$\Pi - \Pi$	690-718	4-53	153	4.7
$\nu_5 + 2\nu_7 - \nu_7$	$\Pi - \Pi$	721-748	2-45	296	4.1
$\nu_5 + \nu_7 - 2\nu_7$	$(\Sigma^+, \Delta) - (\Sigma^+, \Delta)$	290-330	2-81	261	0.9
$\nu_6 + \nu_7 - 2\nu_7$	$(\Sigma^+, \Delta) - (\Sigma^+, \Delta)$	256-306	2-84	402	0.9
$4\nu_7 - 2\nu_7$	$(\Sigma^+, \Delta) - (\Sigma^+, \Delta)$	406-437	5-67	302	1.0

177 ground state transition. This can be seen in Figure 3, where the broad scan covers the $J = 13 \leftarrow 12$
 178 transitions for many vibrational satellites. In this excerpt, the l -type resonance patterns of all the excited
 179 bending states analyzed are visible. From a visual inspection, it is easy to associate some of these patterns to
 180 the pertaining state: the ground and $\nu_4 = 1$ exhibit a single line, while each bending state has $\Sigma = \prod_l (l_t + 1)$
 181 lines (even though not always resolvable).

182 4.3. Analysis of the spectra

183 The sample of pure rotational and ro-vibrational data contains 6691 distinct frequencies involving 14
 184 vibrational states of DC_3N . This work represents the first-ever investigation of its ro-vibrational spectrum
 185 in the region between 365 and 1040 cm^{-1} . Moreover, the FIR spectrum has been thoroughly re-investigated
 186 at higher resolution with an accuracy two or three orders of magnitude better than Ref. [25]. As far as
 187 the rotational spectrum is concerned, this work extends the observation of excited states transitions to

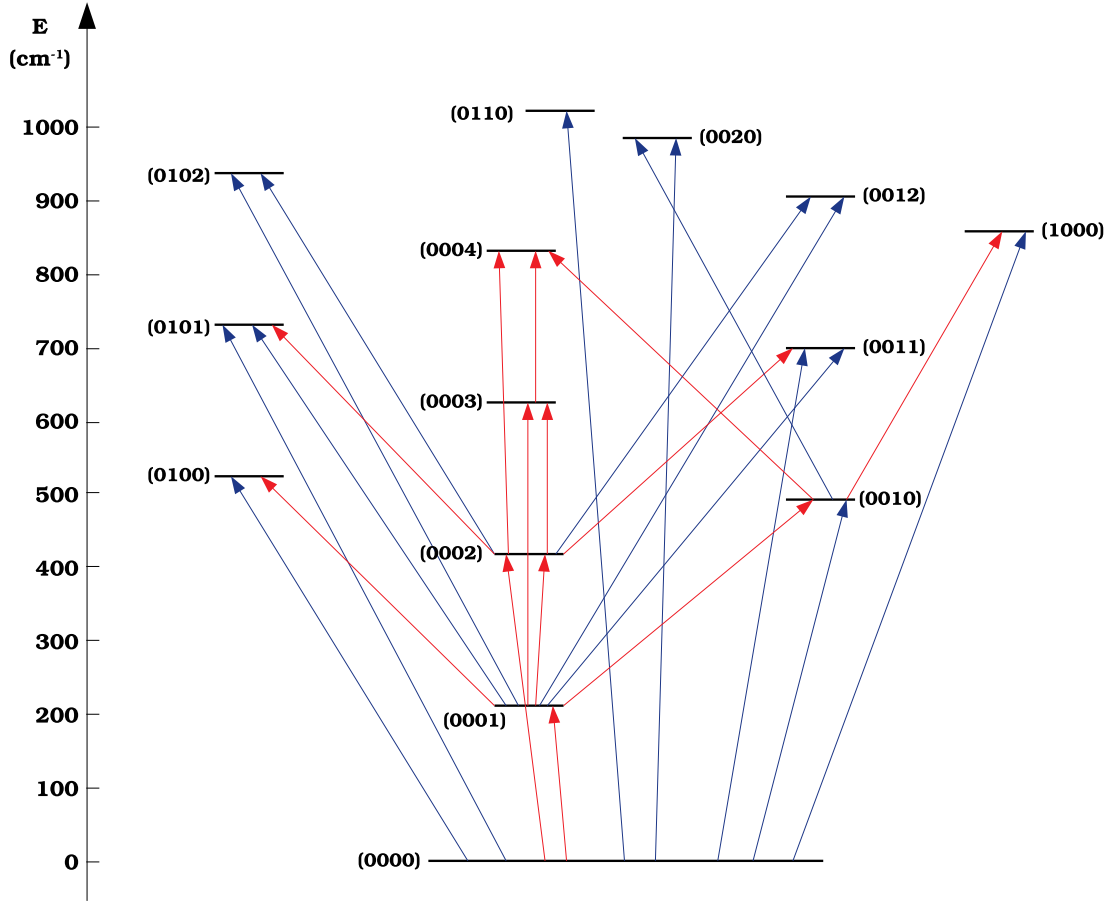


Figure 1: Vibrational energy-level diagram of DC_3N up to 1015 cm^{-1} , where the arrows represent the 27 IR bands analyzed in this work. Red and blue arrows indicate the bands observed at SOLEIL and in Bologna, respectively.

188 the submillimeter-wave region. In addition, rotational transitions with J up to 126 were recorded at THz
 189 frequencies (1.069 THz) although only for the ground state.

190 In the combined fit, a different weight was given to each datum in order to take into account the different
 191 measurements precision. Uncertainties spanning from 0.0004 to 0.00075 cm^{-1} were used for the infrared
 192 measurements performed in Bologna; the weak ν_4 band being the only exception, for which an uncertainty
 193 of 0.001 cm^{-1} was assumed. FIR data recorded at higher resolution with the FT-IR spectrometer of the
 194 AILES beamline have been given uncertainties between 0.00005 and 0.0001 cm^{-1} , based on calibration
 195 residuals and the S/N of spectral lines. As far as pure rotational transitions are concerned, we assumed
 196 a typical experimental error of $10\text{--}20\text{ kHz}$ for our new millimeter/submillimeter measurements. Data from
 197 literature were used with the uncertainty stated in the original papers [17, 18, 19]. Only few lines from
 198 Ref. [17], whose residuals were far off their declared errors, were not used in the fit.

199 The spectral analysis was performed using a custom PYTHON code that employs the SPFIT program
 200 [39] as computational core (see Ref. [38] for further details about the code). The data were fitted to
 201 the Hamiltonian of Eq. (2) and its coefficients optimized in an iterative least-squares procedure. Some
 202 spectroscopic parameters could not be determined from the available experimental data. In these cases, the
 203 constant of a given vibrational level were derived from the corresponding optimized values obtained for other

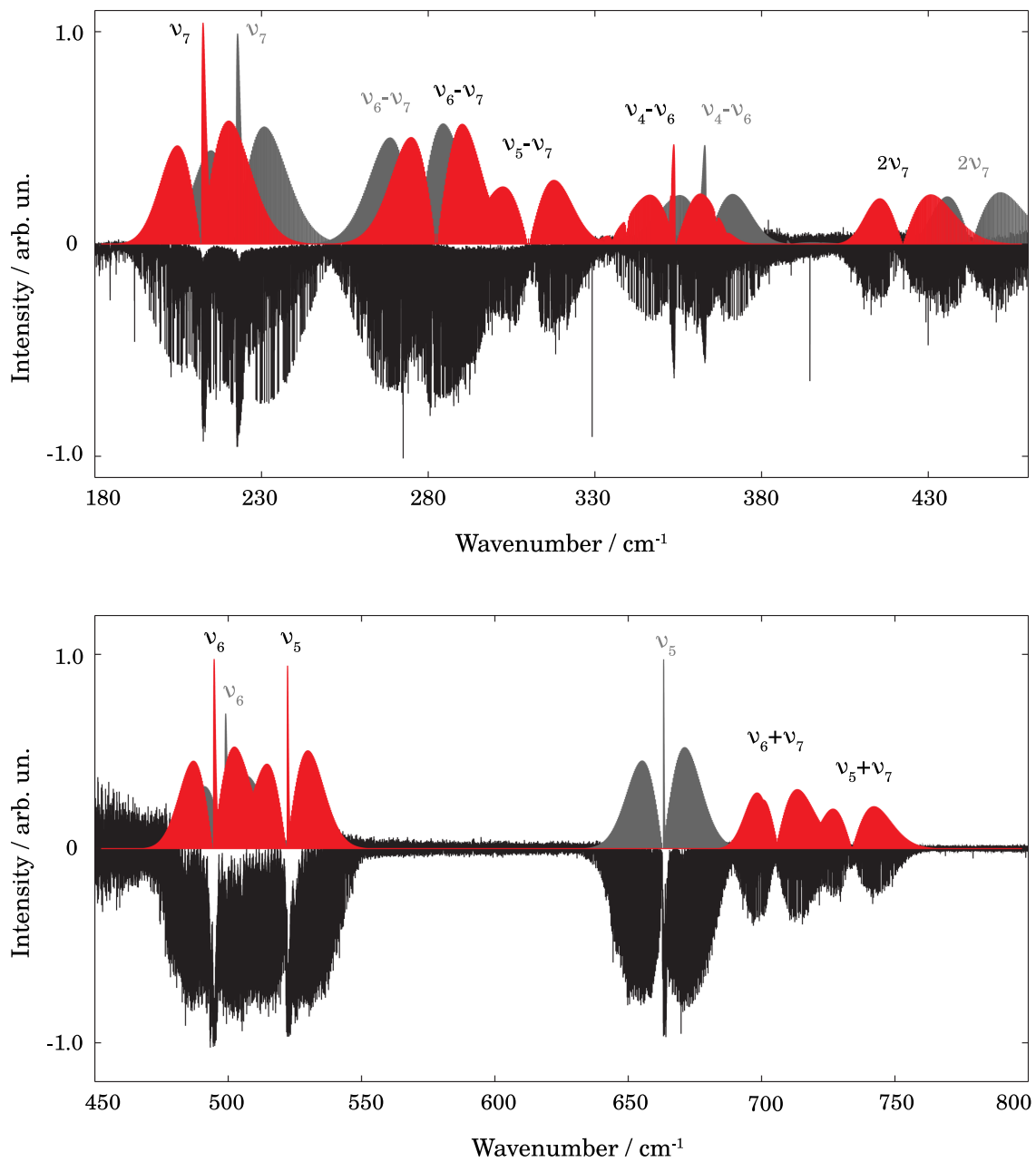


Figure 2: Portions of the FIR (upper panel) and MIR (lower panel) spectra of *d*-cyanoacetylene (black traces). A simulation spectrum of the most intense bands is also reported for both DC₃N (red) and HC₃N (grey). Lines belonging to CO and various H₂O isotopologues were removed from the spectra.

Table 3: Summary of the rotational data used in the analysis.

State	$ k $	J range	Freq. range (GHz)	No. of lines	rms (kHz)	Reference
Ground state	0	3-126	33-1069	52	13.2	TW, Ma78, P188, Sp08
$v_7 = 1$	1 _{e,f}	5-105	50-896	67	10.9	TW, Ma78, P188, Sp08
$v_6 = 1$	1 _{e,f}	7-44	67-381	42	17.0	TW, P188
$v_5 = 1$	1 _{e,f}	7-44	67-381	42	13.7	TW, P188
$v_4 = 1$	0	7-51	67-439	32	23.6	TW, P188
$v_7 = 2$	0, 2 _{e,f}	7-44	67-383	61	24.0	TW, Ma78, P188
$v_7 = 3$	(1, 3) _{e,f}	7-44	68-384	77	20.0	TW, Ma78, P188
$v_7 = 4$	0,(2, 4) _{e,f}	7-48	68-419	85	19.8	TW, P188
$v_6 = 2$	0, 2 _{e,f}	7-44	67-382	54	44.7	TW, P188
$v_6 = v_7 = 1$	(0, 2) _{e,f}	7-44	67-382	93	30.8	TW, Ma78, P188
$v_5 = v_7 = 1$	(0, 2) _{e,f}	7-44	67-382	78	20.8	TW, P188
$v_5 = v_6 = 1$	(0, 2) _{e,f}	9-44	84-381	63	14.6	TW
$v_6 = 1, v_7 = 2$	($\pm 1, 3$) _{e,f}	7-46	68-400	95	21.9	TW, P188
$v_5 = 1, v_7 = 2$	($\pm 1, 3$) _{e,f}	9-44	85-383	97	17.4	TW
interstate ^a		44-49	364-429	10	19.7	TW

Abbreviations are used as follow: **TW** This work, **Ma78** Mallinson & De Zafra (1978) [17], **P188** Plummer *et al.* (1988) [18], **Sp08** Spahn *et al.* (2008) [19]. [a] Transitions between the interacting states (1000) and (0004).

Table 4: Spectroscopic constants derived for DC₃N in the ground and $v_4 = 1$ states.

Constant	Unit	Ground state	$v_4 = 1$
G_v	cm ⁻¹	0.0	867.594(75)
B_v	MHz	4221.580853(37)	4212.271(16)
D_v	kHz	0.4517857(89)	0.45312(11)
H_v	mHz	0.03949(78)	0.03949 ^a
L_v	nHz	-0.154(23)	-0.154 ^a

Number in parenthesis are one standard deviation in units of the last quoted digit. [a] Kept fixed to ground state value.

204 levels belonging to the same vibrational manifold considering, whenever feasible, a vibrational dependence.
 205 In other cases, they were simply fixed to zero. The spectroscopic parameters obtained from the combined
 206 fit procedure are collected in Tables 4,7.

207 As anticipated, the analysis of DC₃N follows the approach successfully adopted for HC₃N [38]. The main
 208 difference is the set-up of the anharmonic resonances network, which arises from the different energy of some
 209 vibrational levels due to the isotopic substitution. In particular, the ν_5 vibrational energy, 663.36848(3) cm⁻¹
 210 in HC₃N, drops to 522.26378(2) cm⁻¹ in DC₃N. For HC₃N, two resonant systems were described: (i) $v_5 =$
 211 $1 \sim v_7 = 3$ and ii) $v_4 = 1 \sim v_5 = v_7 = 1 \sim v_6 = 2 \sim v_7 = 4$. Of the two systems, the former is not present in
 212 DC₃N while the latter is almost the same, except for $v_5 = v_7 = 1$, replaced by $v_5 = v_6 = 1$. The treatment of
 213 such perturbations led to the determination of the corresponding interaction parameters, C_{30} for the cubic

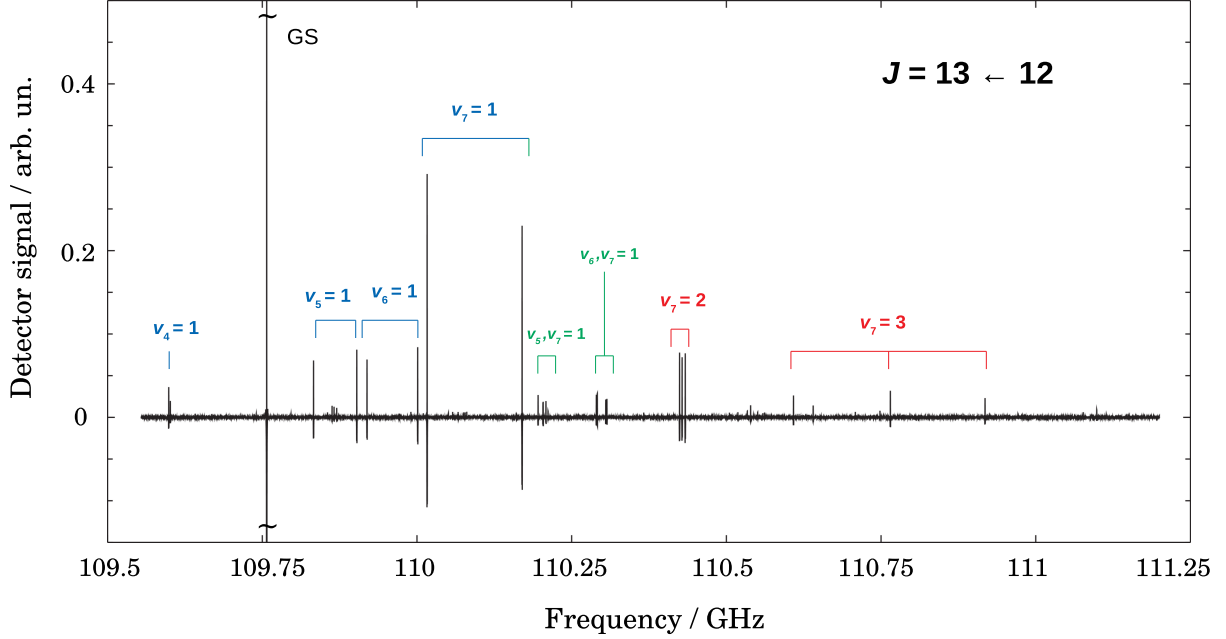


Figure 3: A 2 GHz broad scan of the $J = 13 \leftarrow 12$ rotational transition of DC_3N around 110 GHz. The spectrum was recorded at room temperature, with DC_3N at a pressure of 0.05 Pa, $\text{RC} = 3$ ms, frequency step 50 kHz, $\text{FM} = 120$ kHz, scan speed = 0.4 MHz/s, 2 scans. The arbitrary units of the y -axis are set so that the intensity of the ground state (GS) transition, out of scale in the figure, is 1.

Table 5: Spectroscopic constants derived for DC_3N in singly-excited bending states.

Constant	Unit	$v_7 = 1$	$v_6 = 1$	$v_5 = 1$
G_v	cm^{-1}	211.5502859(33)	492.7605681(48)	522.2639331(49)
$X_{\text{L}(\text{tt})}$	GHz	19.5125 ^a	56.39 ^a	...
B_v	MHz	4234.519466(31)	4229.25208(11)	4225.835835(71)
D_v	kHz	0.4718865(60)	0.462123(45)	0.452490(14)
H_v	mHz	0.08240(30)	0.0637(45)	0.03949 ^b
L_v	nHz	-0.154 ^b	-0.154 ^b	-0.154 ^b
$d_{\text{JL}(\text{tt})}$	kHz	-9.971 ^a	141.5 ^a	...
q_t	MHz	5.907823(56)	3.15095(11)	2.68903(13)
q_{tJ}	Hz	-13.646(11)	-1.572(22)	-1.627(27)
q_{tJJ}	μHz	43.37(57)

Number in parenthesis are one standard deviation in units of the last quoted digit. [a] Constrained value, see text. [b] Kept fixed to ground state value.

214 terms, $(v_4 = 1)-(v_6 = 2)$ and $(v_4 = 1)-(v_5 = v_6 = 1)$, and C_{50} for the quintic term $(v_4 = 1)-(v_7 = 4)$.
 215 Moreover, a centrifugal distortion parameter C_{50}^J was included in the analysis.

216 For the states involved in this resonance system, many experimental data are available. In the MIR
 217 region, we recorded the ν_4 , $\nu_5 + \nu_6$, and $2\nu_6$ bands that provide the energy position for most of the interacting
 218 levels. The energy of the $v_7 = 4$ was determined through the FIR spectrum, where the $4\nu_7 \leftarrow 3\nu_7$ hot-band

Table 6: Spectroscopic constants derived for DC₃N in overtone states.

Constant	Unit	$v_7 = 2$	$v_7 = 3$	$v_7 = 4$	$v_6 = 2$
G_v	cm ⁻¹	422.3753581(61)	632.510162(64)	841.9860892(95)	983.021(78)
$X_{L(tt)}$	GHz	19.354043(62)	19.1988(19)	19.03874(52)	56.39(58)
$y_{L(tt)}$	MHz	1.82(12)	...
B_v	MHz	4247.45224(11)	4260.38118(15)	4273.30576(21)	4236.558(16)
D_v	kHz	0.491827(21)	0.512469(34)	0.53448(11)	0.471993(61)
H_v	mHz	0.03949 ^b	0.03949 ^b	0.176(21)	0.03949 ^b
L_v	nHz	-0.154 ^b	-0.154 ^b	-0.154 ^b	-0.154 ^b
$d_{JL(tt)}$	kHz	-10.426(30)	-10.947(24)	-11.368(21)	141.6(39)
$h_{JL(tt)}$	Hz	-0.0552(64)	...
q_t	MHz	5.93258(10)	5.95888(12)	5.98281(15)	3.15095 ^a
q_{tJ}	Hz	-13.897 ^a	-14.149(36)	-14.288(46)	-1.571 ^a
q_{tJJ}	μHz	43.37 ^a	43.37 ^a	43.37 ^a	...

Number in parenthesis are one standard deviation in units of the last quoted digit. [a] Constrained value, see text. [b] Kept fixed to ground state value.

219 and the $4\nu_7 \leftarrow \nu_6$ band were detected. A large pure rotational data-set is also available for the polyad of
 220 interacting states. Besides several rotational transitions observed within the vibrational states, a small set
 221 of interstate transitions between the (1000) and (0004) states were identified. The coefficients C_{mn} of the
 222 resonance Hamiltonian are given in Table 8.

223 5. Conclusions

224 In this work, a large set of high-resolution rotational and ro-vibrational data of DC₃N has been recorded
 225 and analyzed in order to achieve a detailed knowledge of all the vibrational states approximately below
 226 1000 cm⁻¹ of energy. To reach this goal, infrared spectra of DC₃N have been recorded in the range 150–
 227 1600 cm⁻¹ at high resolution (0.001–0.004 cm⁻¹). In this region, 27 fundamental, overtone, combination, and
 228 hot-bands have been observed and analyzed. Notably, the very weak ν_4 fundamental has also been detected,
 229 even though at lower resolution (0.012 cm⁻¹). Also, pure rotational transitions for 14 states have been
 230 recorded to extend the investigation of the spectrum to the submillimeter-wave region up to *ca.* 500 GHz.

231 Almost 6700 experimental transitions were included in a least-squares fit procedure thanks to which a
 232 large number of rotational and ro-vibrational spectroscopic parameters have been determined for 14 different
 233 vibrational states. The whole set of data has been fitted with an overall weighted standard deviation
 234 σ of 0.95, meaning that on average all data are well-reproduced within their given uncertainties. The
 235 vibrational energies were determined experimentally for all the investigated states, without any assumption.
 236 The combination of both high-resolution ro-vibrational data and pure rotational measurements allowed an
 237 accurate modeling of the spectrum of DC₃N, including perturbations produced by the observed anharmonic
 238 resonances. The interaction between the (1000) and (0110) states has been introduced for the first time,
 239 with the effect to eliminate the residual discrepancies described in Refs. [18, 25].

240 The present work shows once again the success of a combined analysis of data from different spectral
 241 regions, like infrared and millimeter-wave fields. The results are generally more coherent and fewer assump-
 242 tions are needed, if not any. Also, a more extended set of spectroscopic parameters can be obtained with
 243 reliability.

244 This study provides an extensive line catalog (deposited as Supplementary Material) which can be used
 245 to assist future astronomical observations of DC₃N and is suitable for modeling both cold and hot regions

Table 7: Spectroscopic constants derived for DC_3N in combination states.

Constant	Unit	$v_6 = v_7 = 1$	$v_5 = v_7 = 1$	$v_5 = v_6 = 1$	$v_6 = 1, v_7 = 2$	$v_5 = 1, v_7 = 2$
G_v	cm^{-1}	703.8550157(95)	734.058721(13)	1014.2947(11)	914.21137(23)	945.143633(32)
$X_{L_v(\text{aa})}$	GHz	56.39 ^a	56.39 ^a	...
$X_{L_v(\text{bb})}$	GHz	19.3189 ^a	19.5125 ^a	56.39 ^a	19.1254(87)	19.3142(16)
$X_{L_v(\text{ab})}$	GHz	16.16651(21)	23.13131(38)	40.245(33)	16.2848(57)	23.0216(30)
r_{ab}	GHz	-17.04625(41)	0.32219(69)	-63.498(67)	-16.6526(81)	0.87043(34)
r_{abJ}	kHz	-5.784(70)	-65.965(72)	...	-12.0(12)	-64.05(11)
B_v	MHz	4242.274182(83)	4238.741823(94)	4233.55575(16)	4255.2987(20)	4251.64459(18)
D_v	kHz	0.481887(24)	0.472594(28)	0.463447(40)	0.502237(37)	0.492993(33)
H_v	mHz	0.03949 ^b	0.03949 ^b	0.03949 ^b	0.03949 ^b	0.03949 ^b
L_v	nHz	-0.154 ^b	-0.154 ^b	-0.154 ^b	-0.154 ^b	-0.154 ^b
$d_{JL(\text{aa})}$	kHz	-11.254 ^a	141.5 ^a	...
$d_{JL(\text{bb})}$	kHz	141.5 ^a	-9.971 ^a	141.5 ^a	-12.54(76)	-10.482(55)
$d_{JL(\text{ab})}$	kHz	43.88(12)	-5.08(13)	80.35(29)	43.75(46)	-6.810(46)
q_a	MHz	3.17827(15)	2.70634(31)	2.69091(31)	3.19092(20)	2.72654(16)
q_{aJ}	Hz	-1.571 ^a	-1.626 ^a	-1.626 ^a	-1.517 ^a	-1.626 ^a
q_b	MHz	5.94427(18)	5.90943(73)	3.15095 ^a	5.9489(16)	5.93169(23)
q_{bJ}	Hz	-13.646 ^a	-13.738(98)	-1.571 ^a	-14.17(33)	-13.646 ^a
q_{bJJ}	μHz	43.37 ^a	43.37 ^a	...	43.37 ^a	43.37 ^a
v_{ab}	Hz	-1.641(74)

Number in parenthesis are one standard deviation in units of the last quoted digit. [a] Constrained value, see text.
 [b] Kept fixed to ground state value.

Table 8: Resonance parameters.

Interacting states	Parameter	Unit	Value
$(v_4 = 1) - (v_6 = 2)$	C_{30}	cm^{-1}	17.422(33)
$(v_4 = 1) - (v_5 = v_6 = 1)$	C_{30}	cm^{-1}	-6.527(13)
$(v_4 = 1) - (v_7 = 4)$	C_{50}	GHz	2.70065(76)
	C_{50}^J	kHz	9.807(35)

Number in parenthesis are one standard deviation in units of the last quoted digit.

246 of the interstellar medium.

247 6. Acknowledgement

248 This study was supported by Bologna University (RFO funds) and by MIUR (Project PRIN 2015:
 249 STARS in the CAOS, Grant Number 2015F59J3R). This work has been performed under the SOLEIL
 250 proposal #20190128; we acknowledge the SOLEIL facility for provision of synchrotron radiation and would
 251 like to thank the AILES beamline staff for their assistance. L.B., P.C., and B.M.G. acknowledge the support
 252 by the Max Planck Society. V.M.R. has received funding from the European Union’s Horizon 2020 research
 253 and innovation programme under the Marie Skłodowska-Curie grant agreement No 664931. LC acknowledges
 254 support from the Italian Ministero dell’Istruzione, Università e Ricerca through the grant Progetti Premiali
 255 2012 - iALMA (CUP C52I13000140001). J.-C.G. thanks the Centre National d’Etudes Spatiales (CNES)
 256 for a grant.

257 References

- 258 [1] B. A. McGuire, 2018 Census of Interstellar, Circumstellar, Extragalactic, Protoplanetary Disk, and Exoplanetary
 259 Molecules, *Astrophys. J. Suppl. S.* 239 (2018) 17.
- 260 [2] S. Yamamoto, *Introduction to Astrochemistry: Chemical Evolution from Interstellar Clouds to Star and Planet Formation*,
 261 Springer, 2017.
- 262 [3] R. Loomis, et al., The third time’s a charm? a rigorous investigation of spectral line stacking techniques and application
 263 to the detection of HC_{11}N , submitted.
- 264 [4] H. Suzuki, S. Yamamoto, M. Ohishi, N. Kaifu, S.-I. Ishikawa, Y. Hirahara, S. Takano, A survey of CCS, HC_3N , HC_5N ,
 265 and NH_3 toward dark cloud cores and their production chemistry, *Astrophys. J.* 392 (1992) 551–570.
- 266 [5] F. Wyrowski, P. Schilke, S. Thorwirth, K. Menten, G. Winnewisser, Physical conditions in the proto-planetary nebula
 267 CRL 618 derived from observations of vibrationally excited HC_3N , *Astrophys. J.* 586 (1) (2003) 344.
- 268 [6] L. Decin, M. Agúndez, M. J. Barlow, F. Daniel, J. Cernicharo, R. Lombaert, E. De Beck, P. Royer, B. Vandenbussche,
 269 R. Wesson, et al., Warm water vapour in the sooty outflow from a luminous carbon star, *Nature* 467 (7311) (2010) 64.
- 270 [7] J. Li, J. Wang, Q. Gu, Z.-y. Zhang, X. Zheng, Large-scale kinematics, astrochemistry, and magnetic field studies of massive
 271 star-forming regions through HC_3N , HNC, and C_2H mappings, *Astrophys. J.* 745 (1) (2011) 47.
- 272 [8] E. Chapillon, A. Dutrey, S. Guilloteau, V. Piétu, V. Wakelam, F. Hersant, F. Gueth, T. Henning, R. Launhardt,
 273 K. Schreyer, et al., Chemistry in disks. VII. first detection of HC_3N in protoplanetary disks, *Astrophys. J.* 756 (1)
 274 (2012) 58.
- 275 [9] A. J. Al-Edhari, C. Ceccarelli, C. Kahane, S. Viti, N. Balucani, E. Caux, A. Faure, B. Lefloch, F. Lique, E. Mendoza,
 276 et al., History of the solar-type protostar IRAS 16293–2422 as told by the cyanopolyynes, *Astron. Astrophys.* 597 (2017)
 277 A40.
- 278 [10] F. Rico-Villas, J. Martín-Pintado, E. Gonzalez-Alfonso, S. Martín, V. M. Rivilla, Super hot cores in NGC 253: witnessing
 279 the formation and early evolution of super star clusters, *Mon. Not. R. Astron. Soc.* 491 (3) (2020) 4573–4589.
- 280 [11] S. Zeng, I. Jiménez-Serra, V. Rivilla, S. Martín, J. Martín-Pintado, M. Requena-Torres, J. Armijos-Abendaño,
 281 D. Riquelme, R. Aladro, Complex organic molecules in the Galactic Centre: the N-bearing family, *Mon. Not. R. As-*
 282 *tron. Soc.* 478 (3) (2018) 2962–2975.
- 283 [12] W. Langer, F. Schloerb, R. Snell, J. Young, Detection of deuterated cyanoacetylene in the interstellar cloud TMC-1,
 284 *Astrophys. J.* 239 (1980) L125–L128.
- 285 [13] G. B. Esplugues, J. Cernicharo, S. Viti, J. R. Goicoechea, B. Tercero, N. Marcelino, et al., Combined IRAM and Her-
 286 schel/HIFI study of cyano(di)acetylene in Orion KL: tentative detection of DC_3N , *Astron. Astrophys.* 559 (2013) A51.

- [14] A. Belloche, H. Müller, R. Garrod, K. Menten, Exploring molecular complexity with ALMA (EMoCA): Deuterated complex organic molecules in Sagittarius B2 (N2), *Astron. Astrophys.* 587 (2016) A91.
- [15] E. Bianchi, C. Ceccarelli, C. Codella, J. Enrique-Romero, C. Favre, B. Lefloch, Astrochemistry as a tool to follow protostellar evolution: The class I stage, *ACS Earth Space Chem.* 3 (12) (2019) 2659–2674.
- [16] V. M. Rivilla, L. Colzi, F. Fontani, M. Melosso, P. Caselli, L. Bizzocchi, F. Tamassia, L. Dore, DC₃N observations towards high-mass star-forming regions, *Mon. Not. R. Astron. Soc.* Staa1616. [arXiv:https://academic.oup.com/mnras/advance-article-pdf/doi/10.1093/mnras/staa1616/33371666/staa1616.pdf](https://academic.oup.com/mnras/advance-article-pdf/doi/10.1093/mnras/staa1616/33371666/staa1616.pdf), [doi:10.1093/mnras/staa1616](https://doi.org/10.1093/mnras/staa1616). URL <https://doi.org/10.1093/mnras/staa1616>
- [17] P. Mallinson, R. L. de Zafra, The microwave spectrum of cyanoacetylene in ground and excited vibrational states, *Mol. Phys.* 36 (3) (1978) 827–843.
- [18] G. Plummer, D. Mauer, K. Yamada, K. Möller, Rotational spectra of DC₃N in some excited vibrational states, *J. Mol. Spectrosc.* 130 (2) (1988) 407–418.
- [19] H. Spahn, H. S. Müller, T. F. Giesen, J.-U. Grabow, M. E. Harding, J. Gauss, S. Schlemmer, Rotational spectra and hyperfine structure of isotopic species of deuterated cyanoacetylene, DC₃N, *Chem. Phys.* 346 (1-3) (2008) 132–138.
- [20] E. Fliege, H. Dreizler, B. Kleibömer, Deuterium and nitrogen quadrupole coupling in cyanodeuteroacetylene, *J. Mol. Struct.* 97 (1983) 225–228.
- [21] L. Tack, S. G. Kukolich, Beam-maser spectroscopy on cyanoacetylene-D, *J. Chem. Phys.* 78 (11) (1983) 6512–6514.
- [22] M. Uyemura, S. Deguchi, Y. Nakada, T. Onaka, Infrared intensities of bending fundamentals in gaseous HCCCN and DCCCN, *Bull. Chem. Soc. Jpn.* 55 (2) (1982) 384–388.
- [23] Y. Bénilan, A. Jolly, F. Raulin, J.-C. Guillemin, IR band intensities of DC₃N and HC₃¹⁵N: Implication for observations of Titan’s atmosphere, *Planet. Space Sci.* 54 (6) (2006) 635–640.
- [24] P. Mallinson, A. Fayt, High resolution infra-red studies of HCCCN and DCCCN, *Mol. Phys.* 32 (2) (1976) 473–485.
- [25] B. Couveliers, W. Ahmed, A. Fayt, H. Bürger, Far-infrared spectra of DCCCN, *J. Mol. Spectrosc.* 156 (1) (1992) 77–88.
- [26] J.-B. Brubach, L. Manceron, M. Rouzières, O. Pirali, D. Balcon, F. Kwabia-Tchana, V. Boudon, M. Tudorie, T. Huet, A. Cuisset, P. Roy, Performance of the AILES THz-Infrared beamline at SOLEIL for High resolution spectroscopy, in: WIRMS 2009, Vol. 1214 of AIP Conference Proceedings, 2010, pp. 81–84.
- [27] O. Pirali, V. Boudon, J. Oomens, M. Vervloet, Rotationally resolved infrared spectroscopy of adamantane, *J. Chem. Phys.* 136 (2012) 024310.
- [28] O. Pirali, M. Goubet, T. R. Huet, R. Georges, P. Soulard, P. Asselin, J. Courbe, P. Roy, M. Vervloet, The far infrared spectrum of naphthalene characterized by high resolution synchrotron FTIR spectroscopy and anharmonic DFT calculations, *Phys. Chem. Chem. Phys.* 15 (25) (2013) 10141–10150. [doi:10.1039/c3cp44305a](https://doi.org/10.1039/c3cp44305a).
- [29] F. Tamassia, M. Melosso, L. Dore, M. Pettini, E. Canè, P. Stoppa, A. Pietropolli Charmet, Spectroscopy of a low global warming power refrigerant. infrared and millimeter-wave spectra of trifluoroethene (HFO-1123) in the ground and some vibrational excited states, *J. Quant. Spectrosc. Ra.* 248 (2020) 106980. [doi:10.1016/j.jqsrt.2020.106980](https://doi.org/10.1016/j.jqsrt.2020.106980).
- [30] F. Matsushima, H. Odashima, T. Iwasaki, S. Tsunekawa, K. Takagi, Frequency-measurement of pure rotational transitions of H₂O from 0.5 to 5 THz, *J. Mol. Struct.* 352 (1995) 371–378.
- [31] V. M. Horneman, R. Anttila, S. Alanko, J. Pietila, Transferring calibration from CO₂ laser lines to far infrared water lines with the aid of the ν_2 band of OCS and the ν_2 , $\nu_1 - \nu_2$, and $\nu_1 + \nu_2$ bands of ¹³CS₂: Molecular constants of ¹³CS₂, *J. Mol. Spectrosc.* 234 (2) (2005) 238–254.
- [32] I. E. Gordon, L. S. Rothman, C. Hill, R. V. Kochanov, Y. Tan, P. F. Bernath, M. Birk, V. Boudon, A. Campargue, K. Chance, et al., The HITRAN2016 molecular spectroscopic database, *J. Quant. Spectrosc. Ra.* 203 (2017) 3–69.
- [33] C. Degli Esposti, M. Melosso, L. Bizzocchi, F. Tamassia, L. Dore, Determination of a semi-experimental equilibrium structure of 1-phosphapropyne from millimeter-wave spectroscopy of CH₃CP and CD₃CP, *J. Mol. Struct.* 1203 (2020) 127429.
- [34] M. Melosso, L. Dore, F. Tamassia, C. L. Brogan, T. R. Hunter, B. A. McGuire, The sub-millimeter rotational spectrum of ethylene glycol up to 890 GHz and application to ALMA Band 10 spectral line data of NGC 6334I, *J. Phys. Chem. A* 124 (2020) 240–246.
- [35] L. Bizzocchi, V. Lattanzi, J. Laas, S. Spezzano, B. M. Giuliano, D. Prudenzano, C. Endres, O. Sipilä, P. Caselli, Accurate sub-millimetre rest frequencies for HOCO⁺ and DOCO⁺ ions, *Astron. Astrophys.* 602 (2017) A34.
- [36] J. Brown, J. Hougen, K.-P. Huber, et al., The labeling of parity doublet levels in linear molecules, *J. Mol. Spectrosc.* 55 (1-3) (1975) 500–503.
- [37] K. M. Yamada, F. Birss, M. Aliev, Effective Hamiltonian for polyatomic linear molecules, *J. Mol. Spectrosc.* 112 (2) (1985) 347–356.
- [38] L. Bizzocchi, F. Tamassia, J. Laas, B. M. Giuliano, C. Degli Esposti, L. Dore, et al., Rotational and high-resolution infrared spectrum of HC₃N: Global ro-vibrational analysis and improved line catalog for astrophysical observations, *Astrophys. J. Suppl. Ser.* 233.
- [39] H. M. Pickett, The fitting and prediction of vibration-rotation spectra with spin interactions, *J. Mol. Spectrosc.* 148 (2) (1991) 371–377.